Amyloid precursor protein interacts with the mitochondrial phosphatase PGAM5 and regulates mitochondrial respiration

Kriti Shukla[1,2], Zhi Zhang[3], Kendra S. Plafker[1], Satoshi Matsuzaki[1], Casandra Salinas-Salinas[1], Yvonne Thomason[1], Samah Houmam[1,3], Dylan Barber[1,4], Anna Fakye[1,3], Kenneth M. Humphries[1,3], Scott M. Plafker[1], Jialing Lin[3], Heather C. Rice[1,2,3,4]

[1]Aging & Metabolism Research Program, Oklahoma Medical Research Foundation, Oklahoma City, OK, 73104, USA

[2]Department of Chemistry and Biochemistry, University of Oklahoma, Norman, OK, 73072, USA

[3]Department of Biochemistry & Physiology, University of Oklahoma Health Sciences Center, Oklahoma City, OK, 73104, USA

[4]Neuroscience Program, University of Oklahoma Health Sciences Center, Oklahoma City, OK, 73104, USA

Abstract:

Amyloid Precursor Protein (APP) has been reported to partially localize to mitochondria, and mitochondrial dysfunction is a key feature of Alzheimer's disease; however, the mechanisms linking APP to mitochondrial functions remain incompletely defined. In this study, we found that mitochondria isolated from the brains of APP knockout (KO) mice have impaired substrate-specific respiration and electron transport chain function. We identified a novel interaction between APP and phosphoglycerate mutase family member 5 (PGAM5), a mitochondrial phosphatase. We determined that APP and PGAM5 co-localize at mitochondria-ER contact sites (MERCS), and we confirm an endogenous interaction using proximity ligation assays in mouse brain slices. Using in vitro binding assays, we demonstrate a direct interaction between the linker region of APP and a region of PGAM5 that includes the Kelch-like ECH-associated protein 1 (Keap-1) binding domain. PGAM5 is known to anchor a portion of Nuclear respiratory factor 2 (Nrf2) through Keap1 at the outer mitochondrial membrane to regulate the expression of mitochondrial respiratory chain complexes and enzymes. Consistent with this, we found that the Nrf2-regulated genes Hmox1 (Heme oxygenase-1) and Nnqo1 (NADH:quinone oxidoreductase 1), which are involved in mitochondrial respiration, are downregulated in APP KO astrocytes. Together, these findings suggest that APP supports mitochondrial function by

modulating PGAM5-Keap1-Nrf2 signaling, providing a mechanistic link between loss of APP function and impaired mitochondrial respiration.

Introduction:

Alzheimer's disease (AD) is the leading cause of dementia and is pathologically defined by excessive accumulation of amyloid-β (Aβ) plaques and tau tangles in the brain.[1,2] Mitochondrial dysfunction is often considered to be at the nexus of disease onset and above-mentioned pathologies, both in autosomal dominant and sporadic AD.[3–5] Studies have reported altered mitochondrial morphology[6,7], impaired migration[8], increased oxidative stress[5,9,10], dysregulation of mitochondrial enzymes[11], decreased ATP levels[12], impaired brain metabolism and mitochondrial biogenesis in AD conditions[13–15], suggesting the involvement of mitochondrial dysfunction in disease progression.

The Amyloid Precursor Protein (APP) is the parent protein of Aβ peptides that aggregate to form Aβ plaques in Alzheimer's disease.[16,17] Although primarily expressed on the plasma membrane, a portion of APP has been shown to localize to the mitochondria and mitochondria-ER contact sites (MERCS)[18–21]. Various studies have further suggested a functional role of APP in the mitochondria[9,13,22–26]. For instance, APP alters mitochondrial mass, biogenesis, and mitophagy[27]. APP accumulation in the mitochondria prevents the import of oxidative phosphorylation (OXPHOS) subunits, impairing mitochondrial function, while overexpression of APP reduces mitochondrial respiration *in vitro*.[28] There is also strong evidence that MERCS are a site of APP processing[29,30] , and the physical and biochemical apposition of MERCS with mitochondria supports the possibility that APP interacts with mitochondrial proteins to mediate functional outcomes. Despite extensive efforts, it has been challenging to unravel the mechanisms by which APP affects mitochondria; however, understanding its protein-protein interactions can aid understanding its role in the mitochondria [31].

Interestingly, phosphoglycerate mutase family member 5 (PGAM5) was found as a candidate interactor of the APP ectodomain in an unbiased proteomics screen performed by Rice et al. [32]. PGAM5 is a mitochondria-resident protein and acts as a serine-threonine phosphatase towards various protein substrates. PGAM5 regulates mitochondrial dynamics, mitophagy, cell death, redox homeostasis, and mitochondrial respiration.[33–37]. PGAM5 regulates mitochondrial

redox homeostasis and respiration through a nuclear respiratory factor 2 (Nrf2)-dependent pathway[38]. Under homeostatic conditions, Nrf2 is constitutively translated, ubiquitylated by Keap1/Cul3, and degraded by the proteasome[39,40]. A small subset of Nrf2 is tethered to the outer mitochondrial membrane through formation of a ternary complex with PGAM5 and Keap1.[40–42] In response to oxidative stress, modification of cysteines on Keap1 render it enzymatically inactive leading to a halt of the constitutive degradation of Nrf2. Newly synthesized Nrf2 then translocates to the nucleus, where it induces the transcription of antioxidant genes (e.g. *Hmox1 and Nqo1*) to restore redox homeostasis and support mitochondrial respiration[38–40].

In this study, we show that mitochondria from APP KO mouse brains have impaired substrate-specific respiration and electron transport chain function. We establish a novel interaction between APP and the mitochondrial phosphatase PGAM5, where the APP linker region binds PGAM5 within a region containing the Keap1-binding site. Consistent with disrupted PGAM5-Keap1-Nrf2 signaling, expression of the Nrf2 target genes *Hmox1 and Nqo1* are reduced in APP KO astrocytes. Together, these findings suggest a previously unrecognized role for APP in regulating mitochondrial respiration through a PGAM5-Keap1-Nrf2 signaling pathway.

Results:

Mitochondria isolated from APP KO mouse brain have impaired respiration and metabolism

To understand the role of APP in brain mitochondria, we assessed respiration and metabolism in freshly isolated mitochondria from wild-type (WT) vs APP KO mouse brains. As compared to WT, APP KO mitochondria showed significantly decreased pyruvate (Figure 1A) and glutamate-mediated (Figure 1B) respiration with no changes observed in succinate-mediated respiration (Figure 1C) as compared to wild-type, indicating an impairment in maximal NADH-linked mitochondrial respiration whereas Complex II–dependent respiration (succinate) remains intact. Additionally, we measured the effect of APP KO on Complex 1 activity, the rate limiting step of the ETC and NADH oxidase activity as a measure of total ETC activity.[10] Our findings showed a significant decrease in NADH oxidase activity in APP KO mitochondria (Figure 1D) and a decreasing but non-statistically significant trend in complex I activity (Figure

1E). Taken together, these findings suggest that APP plays a role in maintaining Complex I function and NADH-linked oxidative metabolism in brain mitochondria.

APP and PGAM5 colocalize at the mitochondria-ER contact sites and interact with each other both *in vitro* and *ex vivo*

To investigate a potential mechanism for the role of APP in regulating mitochondrial metabolism, we followed up on a proteomics screen performed by Rice et. al showing that PGAM5, a mitochondrial protein, is a candidate interactor of the APP ectodomain[32]. We first looked at the subcellular localization of APP and PGAM5, which would indicate the likeliness of their physical interaction. We performed subcellular fractionation of WT mouse brain to isolate mitochondria, ER, and mitochondria-ER contact sites (MERCS). Consistent with literature, the majority of APP was present in the ER while PGAM5 was predominantly found at the mitochondria (Figure 2A,B). Interestingly, both APP and PGAM5 were found at MERCS (Figure 2A,B), indicating that APP and PGAM5 co-localize and potentially interact at MERCS, suggesting a potential functional role for this interaction at the outer mitochondrial membrane.

Next, we sought to determine whether APP and PGAM5 can directly interact *in vitro*. We used the soluble APP (sAPP) and PGAM5 recombinant proteins (Figure 3A). We performed isothermal titration calorimetry (ITC) assays using these recombinant APP and PGAM5 proteins. ITC revealed a binding interaction with a dissociation constant (K_d) of 3.45 µM between APP and the PGAM5 construct lacking the first 54 amino acids (PGAM5Δ54) (Figure 3A and B). The binding stoichiometry (N = 0.114), consistent with a dodecameric PGAM5 complex associated with an APP dimer. APP is known to form homodimers through its E1 and transmembrane domains, which has been implicated in its processing and function.[43] PGAM5, on the other hand, assembles into higher-order oligomers, predominantly forming dodecamers as well as dimers, that are critical for its functions.[36] Pulldown assays further mapped the binding region. sAPP-Fc effectively pulled down PGAM5Δ54 but not PGAM5Δ90, indicating that the interaction requires PGAM5's N-terminal region containing the Keap1-binding domain (KBD) and multimerization motif (MM) (Figure 3C). Additional pulldown assays using individual APP domains (GFLD, CuBD, ExD, AcD, E2) refined the interacting region, with strongest binding observed for both the acidic (AcD) and extension domain (ExD) of APP (Figure 3D-E).

These results suggest that the linker region of APP (constituted by AcD and ExD domains) and the N-terminal amino acids (aa54-90) of PGAM5 (containing Keap1 binding domain, KBD) are critical for binding between these two proteins.

To understand the physiological relevance of the APP-PGAM5 interaction, we next asked if these proteins associate endogenously in intact brain tissue. APP-PGAM5 interaction was observed in wild-type mouse brain slices, with a pronounced signal that was absent in APP knockout controls, confirming the specificity of the interaction (Figure 4A). Quantification of the PLA signals in the brain slices revealed that this interaction is significantly higher in the cortices as compared to the hippocampus. Furthermore, inside the hippocampus, this interaction is the higher in the SP layer of CA1 region as compared to the SG layer of dentate gyrus (DG) (Figure 4B). These findings establish that APP and PGAM5 not only bind *in vitro* but also interact under physiological conditions in the brain.

Transcription of Nrf2-regulated genes is altered in APP KO astrocytes

To understand the functional implications of binding of APP to the Keap-1 binding domain of PGAM5, we investigated whether the Nrf2-Keap1 pathway is affected by the presence of APP. We examined Nrf2-dependent gene expression in primary astrocytes isolated from the brains of WT or APP KO mice. Astrocytes were chosen based on prior literature demonstrating a critical role for APP in mitochondrial function of astrocytes[44]. Total RNA was isolated from wildtype or APP KO astrocytes and transcript levels of established Nrf2 target genes (*Hmox1, Nqo1, Gclc, Gclm, and Txnrd1*) were quantified by qPCR. Both *Hmox1* and *Nqo1* transcripts were significantly reduced in APP KO astrocytes compared to wild-type controls, whereas no significant differences were observed for *Gclc*, *Gclm*, or *Txnrd1* (Figure 5). Reduced basal expression of the Nrf2 targets NQO1 and HO-1 provides a mechanistic link between impaired PGAM5-Keap1-Nrf2 signaling and the selective loss of NADH-linked respiration (as seen in Figure 1), as both enzymes are essential for sustaining redox conditions that permit efficient NADH oxidation at Complex I.[45,46] Together, these data support a model in which APP contributes to efficient basal activation of Nrf2 by regulating PGAM5-Keap1 interactions at the mitochondrial surface through its binding with PGAM5.

Discussion

Mitochondrial dysfunction is widely recognized as a hallmark of Alzheimer's disease (AD), yet the upstream mechanisms driving these defects during disease progression remain poorly defined. Although numerous studies have implicated amyloid precursor protein (APP) in mitochondrial impairment under pathological conditions, its physiological role within mitochondria has been less explored. Understanding how APP functions in healthy mitochondria may therefore provide critical insight into the primary processes that initiate mitochondrial dysfunction and identify points of intervention that could slow or prevent disease progression.

In this study, we show that APP deficiency leads to a selective reduction in glutamate- and pyruvate-driven respiration. This substrate-specific defect points to a dysfunction upstream of or at Complex I, rather than a global failure of the electron transport chain or mitochondrial integrity. Consistent with this interpretation, we also observe a reduction in NADH oxidase activity and a downward trend in Complex I enzymatic activity in APP knockout mitochondria. Together, these results position APP as a previously unappreciated regulator of NADH-linked oxidative metabolism in the brain. In summary, these results demonstrate that loss of APP compromises mitochondrial respiration and reduces electron transport capacity required for sustained energy production. These findings establish APP as an essential contributor to mitochondrial bioenergetics under basal conditions and suggest that mitochondrial dysfunction observed in AD may, in part, reflect a loss of normal APP function rather than solely a gain of toxic amyloid-related effects.

We also show that under physiological conditions, not only APP and a mitochondrial phosphatase PGAM5 colocalize at MERCS, but they also bind directly *in vitro* with micromolar affinity. We also confirmed the endogenous interaction between these two proteins in the brain in a region- and layer-specific manner. The interaction requires the N-terminal region of PGAM5 containing the Keap1-binding domain, indicating that APP might compete with Keap1 for its binding to PGAM5 and in turn, help regulate certain mitochondrial processes. PGAM5 is known to function as a scaffold to tether Nrf2 at the outer mitochondrial membrane via a ternary complex (PGAM5-Keap1-Nrf2). Based on our findings, we propose a model in which APP facilitates efficient Nrf2 activation by modulating PGAM5-Keap1 interactions at the outer mitochondrial membrane. APP binding to PGAM5 may promote displacement of Keap1-bound

Nrf2, enabling Nrf2 stabilization and nuclear translocation (Figure 6). Loss of APP disrupts this signaling platform, resulting in insufficient antioxidant and redox buffering capacity, increased vulnerability of Complex I to oxidative inhibition, and impaired NADH oxidation. This model integrates APP into mitochondrial stress signaling, expanding its functional roles in the healthy brain and provides a mechanistic basis for mitochondrial bioenergetic deficits observed upon APP loss.[47–49]

Consistent with this model, we find that transcription of specific Nrf2 target genes is altered in APP KO primary astrocytes. Under basal conditions, expression of *Nqo1* and *Hmox1* is significantly reduced, and *Nqo1* remains suppressed following oxidative challenge. Importantly, both NQO1 and HO-1 are critical components of the Nrf2 antioxidant network that preserve mitochondrial redox homeostasis.[50] NQO1 limits quinone redox cycling and supports NAD^+/NADH balance, while HO-1- derived metabolites mitigate oxidative stress and protect redox-sensitive mitochondrial enzymes.[51–54] Reduced expression of these genes provides a mechanistic link between APP–PGAM5 interaction and the loss of NADH-linked respiration observed in APP-deficient mitochondria.

Lastly, these observations were made under physiological conditions, independent of overt AD pathology. This underscores a critical gap in current understanding of APP biology prior to symptom onset and suggests that disruption of its normal mitochondrial functions may represent an early and underappreciated contributor to neurodegeneration. Restoring or preserving the physiological roles of APP, particularly in mitochondrial respiration and redox homeostasis, may therefore represent a promising therapeutic strategy for Alzheimer’s disease.

Materials and Methods

Mouse models

All experiments were conducted following a protocol approved by the Oklahoma Medical Research Foundation's (OMRF) Institutional Animal Care and Use Committee prior to any animal work. Genetically modified mouse strain used in this study was APP-KO (strain 004113, B6.129S7-App/J, The Jackson Laboratory). Both C57BL/6J and APP KO mice (The Jackson Laboratories) were group housed in the AALAS-accredited OMRF vivarium on a 14:10 h

light/dark cycle with *ad libitum* access to water and food. The homozygosity of the strains was confirmed by genotyping ear-punch biopsies via Transnetyx.

Respiratory measurements with isolated mitochondria

Freshly isolated mouse brain mitochondria were resuspended in mitochondrial resuspension buffer (250 mM mannitol, 5 mM HEPES, pH 7.4, and 0.5 mM EGTA) as previously described.[55] The protein quantification was done via BCA assay. Mitochondrial respiration measurements were performed according to established protocols.[56] Briefly, mitochondria were diluted to a final concentration of 0.25 mg/mL in respiration buffer containing 210 mM mannitol, 70 mM sucrose, 10 mM MOPS, and 5 mM KH_2PO_4 (pH 7.4). Substrate-driven respiration was assessed using either 0.1 mM pyruvate plus 1 mM malate, 10 mM glutamate plus 1 mM malate, or 1 mM succinate. Oxygen consumption was measured using a fluorescence lifetime–based dissolved oxygen monitoring system (Instech) at 20°C. State 3 respiration was initiated by the addition of ADP (0.5 mM) at 2 min, and oxygen consumption was monitored until complete conversion of ADP to ATP, corresponding to state 4 respiration.

ETC enzyme activity assays

NADH oxidase activity was measured as previously described.[57] Briefly, isolated and protein quantified mitochondria were snap frozen in 25 mM MOPS (pH 7.4) at 0.025 mg/mL and kept in liquid nitrogen until ready to be used. To this frozen-thawed solution, 150 μM NADH was added and the rotenone-sensitive rate of NADH oxidation (ε_{340} = 6200 M^{-1} cm^{-1}) was measured spectrophotometrically via an Agilent 8453 diode array UV−Vis spectrophotometer. To measure Complex 1 activity, 150 μM NADH was added to the frozen-thawed mitochondria, followed by 10mM KCl. Complex I activity was monitored spectrophotometrically as the rate of NADH oxidation. Rotenone (100 nM) was used as an inhibitor to ensure NADH utilization was dependent on complex I activity.

Plasmids

Fc-tagged constructs of APP fragments were provided by Dr. Bart De Strooper and Dr. Joris de Wit (VIB-KU Leuven, Belgium). These were previously generated by PCR-amplifying the following regions of mouse APP_{695}: sAPPα (18-612aa); GFLD (18-128aa); CuBD (129-194aa); AcD-Exd (195-298aa); ExD (195-227aa); AcD (228-298aa); and E2 (299-494aa). Each of the

PCR fragments were inserted in frame between the prolactin signal peptide and human Fc sequence in the pCMV6-XL4 vector using Gibson Assembly (NEB). PGAM5 plasmids were received from Apirat Chaikuad (chaikuad@pharmchem. uni-frankfurt.de).

Purification of recombinant soluble APP proteins

APP fragments with a C-terminal Fc tag were expressed by transfection in HEK293T cells using polyethylenimine (PEI) (Kyfora Bio 23966) and collected in serum-free Opti-MEM media (Gibco 31985088). For Fc-tagged proteins used in proteomics screens and *in vitro* binding assays, the conditioned medium was applied to an affinity column packed with Protein-G Sepharose Fast Flow resin (Cytiva 17061802) at 4 °C at a flow rate ~50mL/hr, washed with 250 mL wash buffer (50 mM HEPES pH 7.4, 300 mM NaCl) and eluted with 10 mL of IgG elution buffer (Pierce). For non-Fc-tagged proteins used in ITC, the conditioned medium was passed through a Protein-G Sepharose Fast Flow column, followed by washing with 250 mL of wash buffer (50 mM Tris pH 8.0, 450 mM NaCl, 1 mM EDTA). The Fc tag was cleaved by overnight incubation with GST-tagged 3C PreScission Protease (Cytiva 27084301) in cleavage buffer (50mM Tris pH 8.0, 150 mM NaCl, 1 mM EDTA, 1 mM DTT). Cleaved protein was collected in the eluate and the protease separated from the eluted proteins using a Glutathione Sepharose (Cytiva 17513201) column collecting in TNE buffer (50mM Tris pH 8.0, 150 mM NaCl, 1 mM EDTA). Proteins were dialyzed against suitable buffer, concentrated using centrifugal filter units (Millipore Sigma UFC9010), and depleted of endotoxin with Pierce™ High-Capacity Endotoxin Removal Spin Columns (Thermo Scientific 88274). Protein concentration was determined by BCA Protein Assay (Thermo Scientific 23227) and verified by Coomassie SDS-PAGE.

Purification of recombinant soluble PGAM5 proteins

PGAM5 plasmids were transfected in BL21 Rosetta competent cells for expression and plated on LB+Kanamycin$^{25ug/ml}$ plate and left overnight at 37°C. Next day, 25ml of LB+Kanamycin$^{25ug/ml}$ was inoculated with a few colonies from this overnight plate and left in a shaker incubator (37°C, 250rpm) overnight. Next day, 10ml of this culture was used to inoculate 500ml of LB+Kanamycin$^{25ug/ml}$ (37°C, 250rpm) for a few hours until the OD reached 0.6-0.8. Protein expression was induced by adding 0.5mM IPTG and incubating for 18hrs (18°C, 225rpm). Cells were harvested by centrifugation and re-suspended in 15ml of lysis

buffer (50mM Hepes-KOH$^{7.5}$, 500mM NaCl, 5mM Imidazole, 5% glycerol with fresh 0.5mM TCEP, 1XPIM (200X: 976ul of H_2O, 20ul of 1.5mg/ml-Aprotinin, 2ul of 10mg/ml-Pepstain, 2ul of 10mg/ml-Leupeptin,) 0.5mM PMSF). Cells were then sonicated (60% power, 3min/cycle, total 4-5 cycles) in the presence of 40ug/ml of DNAse. Supernatant was collected and incubated with 1ml of 50% Ni-beads (rock, 4°C, 2-3 hours). Ni+/supernatant mixture was passed through the column and washed with lysis buffer (10mM imidazole pH 7.4 with 0.5mMTCEP, 1XPIM, 0.2mMPMSF). Protein was eluted with lysis buffer containing higher imidazole concentration (250mM imidazole with 0.5mM TECP). Protein was concentrated to OD280 ~10-15 by using MWCO 10kDa concentrator and quantified using BCA assay. The purified proteins were dialyzed in 1X PBS, pH 7.4 and frozen at -80°C after adding glycerol to a final concentration of 20% (v/v), for subsequent experiments.

Protein pull-down assays

3 µg of Fc tagged-sAPPα (~95KD) was incubated with either 3 µg PGAM5-ΔN90 (25KD) or PGAM5-ΔN54 (30KD) in 500 µL binding buffer (10mM HEPES pH 7.4, 150mM NaCl, 2mM CaCl2, 1mM MgCl2, 0.1% Tween-20) at 4□°C for 1 hour with gentle rotation. For pull-down, 20ul of protein G beads, pre-equilibrated with cold binding buffer, were added and incubated for an additional 2 hours at 4□°C. Afterwards, flow-through was collected and the beads were washed 3–4 times at 3000rpm for 2 min with 500µl binding buffer to remove non-specifically bound proteins. Proteins bound to the beads were eluted in 25ul of SDS sample buffer, supplemented by 10% β-mercaptoethanol, heated at 95°C for 5 minutes and resolved on 13% SDS-PAGE gels, along with the flow-through samples. Gels were then incubated for 1 hour at RT with the Coomassie stain and then washed with DI water (3 times, 15 min each at RT). The gels were then imaged using white light in Syngene™ G:Box apparatus to visualize the protein bands.

Isothermal Titration Calorimetry

All ITC experiments were performed on a MicroCal PEAQ-ITC system at OU Protein Production and Characterization Core. For experiments involving APP constructs expressed in HEK293T cells, the purified PGAM5 and sAPPα constructs were dialyzed into a buffer containing 20 mM Na-HEPES pH 7.0, 150 mM NaCl, and 5 mM $MgCl_2$. Dialyzed samples were concentrated and degassed prior to the experiment. In these experiments, sAPPα were placed

in the sample cell, with matching buffer in the reference cell. PGAM5 constructs were loaded into the syringe and injected into the sample cell in a series of 1 µL injections at 25°C. The raw ITC data were fitted to a single binding site model using the MicroCal PEAQ-ITC analysis software provided by the manufacturer.

Fractionation of mouse brain to isolate subcellular compartments

Brain mitochondria and mitochondria-ER contact sites (MERCS) were isolated from adult mouse brains using a modified version of the protocol by Wieckowski et al. (2009)[55]. Briefly, freshly dissected brains were homogenized in ice-cold isolation buffer containing 0.25 M sucrose, 10 mM HEPES (pH 7.4), and protease inhibitors. The homogenate was subjected to sequential centrifugation to remove nuclei and debris, followed by differential centrifugation steps to separate crude mitochondria. A Percoll density gradient was used to purify mitochondria, and the post-mitochondrial supernatant was further processed to isolate MERCS. All steps were performed at 4°C to preserve organelle integrity.

Western Blotting

Samples obtained from subcellular fractionation were quantified using the BCA protein assay (Thermo Fisher Scientific). 12 µg of protein sample was loaded on each lane, mixed with 10x reducing agent and 4X Laemmli sample buffer, boiled for 5 minutes at 95°C, and resolved on NuPAGE™ 4-12% Bis-Tris Midi gels with MES SDS running buffer. Proteins were transferred onto nitrocellulose membranes (BioRad) using Criterion Blotter (BioRad) at 400mA for 80 minutes. Membranes were blocked with 5% BSA in water for 1 hour at room temperature and then incubated overnight at 4°C with primary antibodies diluted 1:1000 in 0.05% Tween-20 in PBS (PBST)- APPY188 (rabbit, abcam, ab32136), PGAM5 (rabbit, abcam, ab126534), TOM20 (rabbit, Thermo-Fisher, 11802-1-AP), ATPase (mouse, Sigma-Aldrich, 05-369-25UG), BiP (rabbit, abcam, ab108613). After washing three times with PBST, membranes were incubated with secondary antibodies (Alexa Flour™ Donkey anti-Rabbit 800 and Donkey anti-Mouse 680) for 1 hour at room temperature. Protein bands were visualized using Odyssey CLx detection system (Licor). The gel image was converted to grayscale, and the protein and background band intensities were obtained using ImageJ software The background intensity was then used to normalize the protein band intensity, and these values were plotted as protein levels in each subcellular compartment.

Primary Mouse Astrocyte Culture

Primary astrocytes were isolated from whole brains of postnatal day 0–5 (P0–P5) C57BL/6J mice using a differential adhesion–based protocol (cite Güler et al., 2021 https://pubmed.ncbi.nlm.nih.gov/34917973/). All dissections were performed under sterile conditions. Brains were rapidly removed, transferred to ice-cold Hank's Balanced Salt Solution (HBSS), and meninges were carefully stripped to minimize contamination from fibroblasts and endothelial cells. Cortical tissue was mechanically dissociated and enzymatically digested to generate a single-cell suspension. Briefly, 0.05% DNase I was added to the tissue, followed by gentle trituration 10–15 times. Subsequently, 0.05% trypsin was added, and the tissue was further triturated 20–30 times using a 10 mL pipette before incubation at room temperature (22–25 °C) for 20 min. Cells were centrifuged for 10 min at 150 × g, resuspended in complete Dulbecco's Modified Eagle Medium (DMEM) supplemented with 10% fetal bovine serum and penicillin–streptomycin, and plated. The cells were cultured in the astrocyte media and maintained at 37°C with 5% CO_2. Media was changed on day 2 and subsequently every 2–3 days until they reached desired confluency. These were then either used for experiments or flash frozen for future use.

Immunohistochemistry

Mice were transcardially perfused with 1X PBS to remove blood followed by 4% paraformaldehyde. Brains were dissected, post fixed with 4% paraformaldehyde for 1 hour, cryopreserved in 30% sucrose solution, and embedded in Tissue-Tek® OCT for freezing. Coronal cryosections were prepared with 20µm thickness. Sections were permeabilized and blocked at RT for 2 hours in PBS, 0.5% Triton X-100, 5% normal horse serum, and incubated with the primary antibody at 4˚C overnight followed by 2 hours incubation with fluorophore-conjugated secondary antibodies. The following primary antibodies were used- APPY188 Rb (Abcam, ab32136) and PGAM5 Rb (Abcam, ab126534). Fluorophore-conjugated secondary antibodies were from Jackson Immuno, Licor or ThermoFisher. Images were acquired by confocal microscopy with Leica LSM 880 Airyscan.

Proximity ligation assay

Brains from adult wild-type (WT) and APP knockout (APP-KO) mice were harvested following transcardial perfusion with 1X PBS followed by 4% paraformaldehyde (PFA). Brains were post-

fixed in 4% PFA for 1 hour at 4 °C, then cryoprotected in 30% sucrose in PBS until fully equilibrated (indicated by full submersion in sucrose). Tissue was embedded in OCT compound and frozen on dry ice. Coronal sections (20 µm) were cut using Cryotome Leica 3050 and mounted onto microscope slides. Sections were stored at -20 °C until staining. For proximity ligation assay (PLA), sections were brought to room temperature, permeabilized with 0.3% Triton X-100 in PBS for 30 min, and blocked using Duolink® Blocking Solution (Sigma-Aldrich) for 1 h at 37 °C in a humidity chamber. Primary antibodies (rabbit anti-APP and mouse anti-PGAM5) were diluted 1:200 in Duolink® Antibody Diluent and incubated overnight at 4 °C. The following day, sections were incubated with species-specific PLA probes (PLUS anti-rabbit and MINUS anti-mouse, Sigma-Aldrich) for 1 h at 37 °C. Ligation and amplification were performed using the Duolink® In Situ Far Red Detection Kit, according to the manufacturer's protocol. Sections were mounted with Duolink® Mounting Medium and imaged using confocal microscopy at 63x oil-immersion lens.

qPCR

Wild-type (WT) and APP KO mice primary astrocytes were treated with 25 µM tBHQ for 8 hours at 37 °C. The control cells were treated with 20% ethanol (vehicle). Total RNA was extracted from these cells using the Direct-zol micro RNA isolation kit (Zymo Research) and quantified using a Nanodrop 1000 spectrophotometer. 0.25 µg RNA was used to synthesize cDNA using qScript (Quanta) according to manufacturer instructions in a BioRad T100 thermocycler. Real-time quantitative PCR was performed using PowerUp™ SYBR® Green PCR Master Mix (Applied Biosystems) and the primers for the genes- *Hmox1, Nqo1, Gclc, Gclm*, *Txnrd1* and *Actb.* The mRNA levels of target genes were normalized to *ActB* by untreated WT sample values.

Acknowledgements

This work was supported by the National Institutes of Health (R35GM142726, P20GM125528 to H.C.R.) and the Presbyterian Health Foundation (Pilot Research Funding to H.C.R.). The Isothermal Calorimetry experiments were done at OU Protein Production and Characterization Core facility, supported by Institutional Development Awards (IDeA) from the National Institute of General Medical Sciences of the National Institutes of Health (Grants P20GM103640 and P30GM145423), the OU Vice President for Research and Partnerships, and the OU College of

Arts and Sciences. Data processing and analysis were supported by the OMRF Center for Biomedical Data Sciences and the Confocal imaging was done at the OMRF Imaging Core. Figure 6 schematic was created in BioRender.

Bibliography

1. Alzheimer's Disease Fact Sheet | National Institute on Aging. https://www.nia.nih.gov/health/alzheimers-and-dementia/alzheimers-disease-fact-sheet.
2. Serrano-Pozo, A., Frosch, M. P., Masliah, E. & Hyman, B. T. Neuropathological alterations in Alzheimer disease. *Cold Spring Harb. Perspect. Med.* 1, (2011).
3. Pszczołowska, M. *et al.* Mitochondrial disorders leading to Alzheimer's disease—perspectives of diagnosis and treatment. *GeroScience* vol. 46 2977–2988 Preprint at https://doi.org/10.1007/s11357-024-01118-y (2024).
4. Ashleigh, T., Swerdlow, R. H. & Beal, M. F. The role of mitochondrial dysfunction in Alzheimer's disease pathogenesis. *Alzheimer's and Dementia* 19, 333–342 (2023).
5. Misrani, A., Tabassum, S. & Yang, L. Mitochondrial Dysfunction and Oxidative Stress in Alzheimer's Disease. *Frontiers in Aging Neuroscience* vol. 13 Preprint at https://doi.org/10.3389/fnagi.2021.617588 (2021).
6. Trimmer, P. A. *et al.* Abnormal mitochondrial morphology in sporadic Parkinson's and Alzheimer's disease cybrid cell lines. *Exp. Neurol.* 162, 37–50 (2000).
7. Wang, X. *et al.* Impaired Balance of Mitochondrial Fission and Fusion in Alzheimer's Disease. *The Journal of Neuroscience* 29, 9090 (2009).
8. Knott, A. B., Perkins, G., Schwarzenbacher, R. & Bossy-Wetzel, E. Mitochondrial fragmentation in neurodegeneration. *Nat. Rev. Neurosci.* 9, 505–518 (2008).
9. Dumont, M. *et al.* Reduction of oxidative stress, amyloid deposition, and memory deficit by manganese superoxide dismutase overexpression in a transgenic mouse model of Alzheimer's disease. *The FASEB Journal* 23, 2459 (2009).
10. Wang, J., Xiong, S., Xie, C., Markesbery, W. R. & Lovell, M. A. Increased oxidative damage in nuclear and mitochondrial DNA in Alzheimer's disease. *J. Neurochem.* 93, 953–962 (2005).
11. Mastrogiacomo, F., Lindsay, J. G., Bettendorff, L., Rice, J. & Kish, S. J. Brain protein and alpha-ketoglutarate dehydrogenase complex activity in Alzheimer's disease. *Ann. Neurol.* 39, 592–598 (1996).
12. Zhang, C., Rissman, R. A. & Feng, J. Characterization of ATP Alternations in an Alzheimer's Transgenic Mouse Model. *J. Alzheimers Dis.* 44, 375 (2015).
13. Gasparini, L. *et al.* Energy metabolism inhibition impairs amyloid precursor protein secretion from Alzheimer's fibroblasts. *Neurosci. Lett.* 263, 197–200 (1999).

14. Li, P. A., Hou, X. & Hao, S. Mitochondrial biogenesis in neurodegeneration. *J. Neurosci. Res.* 95, 2025–2029 (2017).

15. Singulani, M. P. *et al.* Impairment of PGC-1α-mediated mitochondrial biogenesis precedes mitochondrial dysfunction and Alzheimer's pathology in the 3xTg mouse model of Alzheimer's disease. *Exp. Gerontol.* 133, (2020).

16. Glenner, G. G. & Wong, C. W. Alzheimer's disease: Initial report of the purification and characterization of a novel cerebrovascular amyloid protein. *Biochem. Biophys. Res. Commun.* 120, 885–890 (1984).

17. Masters, C. L. *et al.* Amyloid plaque core protein in Alzheimer disease and Down syndrome. *Proc. Natl. Acad. Sci. U. S. A.* 82, 4245 (1985).

18. Devi, L., Prabhu, B. M., Galati, D. F., Avadhani, N. G. & Anandatheerthavarada, H. K. Accumulation of Amyloid Precursor Protein in the Mitochondrial Import Channels of Human Alzheimer's Disease Brain Is Associated with Mitochondrial Dysfunction. *The Journal of Neuroscience* 26, 9057 (2006).

19. Anandatheerthavarada, H. K., Biswas, G., Robin, M. A. & Avadhani, N. G. Mitochondrial targeting and a novel transmembrane arrest of Alzheimer's amyloid precursor protein impairs mitochondrial function in neuronal cells. *Journal of Cell Biology* 161, 41–54 (2003).

20. Area-Gomez, E. *et al.* Upregulated function of mitochondria-associated ER membranes in Alzheimer disease. *EMBO J.* 31, 4106–4123 (2012).

21. Bhattacharyya, R. *et al.* Axonal generation of amyloid-β from palmitoylated APP in mitochondria-associated endoplasmic reticulum membranes. *Cell Rep.* 35, (2021).

22. Gabuzda, D., Busciglio, J., Chen, L. B., Matsudaira, P. & Yankner, B. A. Inhibition of energy metabolism alters the processing of amyloid precursor protein and induces a potentially amyloidogenic derivative. *Journal of Biological Chemistry* 269, 13623–13628 (1994).

23. Wilkins, H. M. & Swerdlow, R. H. Amyloid precursor protein processing and bioenergetics. *Brain Res. Bull.* 133, 71–79 (2017).

24. Strope, T. A. & Wilkins, H. M. Amyloid Precursor Protein and Mitochondria. *Curr. Opin. Neurobiol.* 78, 102651 (2023).

25. Strope, T. A. & Wilkins, H. M. The reciprocal relationship between amyloid precursor protein and mitochondrial function. *J. Neurochem.* 168, 2275–2284 (2024).

26. Strope, T. A. *et al.* Amyloid-β protein precursor modulates mitophagy and mitochondrial function through its cellular localization. *Journal of Alzheimer's Disease* https://doi.org/10.1177/13872877251360243/SUPPL_FILE/SJ-DOCX-1-ALZ-10.1177_13872877251360243.DOCX (2025) doi:10.1177/13872877251360243/SUPPL_FILE/SJ-DOCX-1-ALZ-10.1177_13872877251360243.DOCX.

27. Wilkins, H. M. Mitochondrial Localized Amyloid Precursor Protein Alters Mitochondrial Function and Mitophagy. *Alzheimer's & Dementia* 19, e074226 (2023).

28. Lopez Sanchez, M. I. G. *et al.* Amyloid precursor protein drives down-regulation of mitochondrial oxidative phosphorylation independent of amyloid beta. *Sci. Rep.* 7, (2017).

29. Del Prete, D. *et al.* Localization and Processing of the Amyloid-β Protein Precursor in Mitochondria-Associated Membranes. *Journal of Alzheimer's Disease* 55, 1549 (2017).

30. Schreiner, B., Hedskog, L., Wiehager, B. & Ankarcrona, M. Amyloid-β Peptides are Generated in Mitochondria-Associated Endoplasmic Reticulum Membranes. *Journal of Alzheimer's Disease* 43, 369–374 (2015).

31. Rice, H. C. *et al.* Secreted amyloid-b precursor protein functions as a GABA B R1a ligand to modulate synaptic transmission. *Science (1979).* 363, (2019).

32. Rice, H. C. *et al.* Secreted Amyloid-β Precursor Protein Functions as a GABABR1a Ligand to Modulate Synaptic Transmission. *Science* 363, (2019).

33. Lu, W. *et al.* Mitochondrial Protein PGAM5 Regulates Mitophagic Protection against Cell Necroptosis. *PLoS One* 11, e0147792 (2016).

34. Yu, B. *et al.* Mitochondrial phosphatase PGAM5 modulates cellular senescence by regulating mitochondrial dynamics. *Nature Communications 2020 11:1* 11, 1–17 (2020).

35. Okuno, H. *et al.* Lipin-1 is a novel substrate of protein phosphatase PGAM5. *Biochem. Biophys. Res. Commun.* 509, 886–891 (2019).

36. Sekine, S. *et al.* Rhomboid protease PARL mediates the mitochondrial membrane potential loss-induced cleavage of PGAM5. *J. Biol. Chem.* 287, 34635–34645 (2012).

37. Ma, K. *et al.* Dynamic PGAM5 multimers dephosphorylate BCL-xL or FUNDC1 to regulate mitochondrial and cellular fate. *Cell Death & Differentiation 2019 27:3* 27, 1036–1051 (2019).

38. Safakli, R. N., Gray, S., Bernardi, N. & Smyrnias, I. Unveiling a novel signalling pathway involving NRF2 and PGAM5 in regulating the mitochondrial unfolded protein response in stressed cardiomyocytes. *Int. J. Biochem. Cell Biol.* 178, 106704 (2025).

39. Zeb, A. *et al.* A novel role of KEAP1/PGAM5 complex: ROS sensor for inducing mitophagy. *Redox Biol.* 48, 102186 (2021).

40. Baird, L. & Yamamoto, M. The Molecular Mechanisms Regulating the KEAP1-NRF2 Pathway. *Mol. Cell. Biol.* 40, e00099-20 (2020).

41. Lo, S. C. & Hannink, M. PGAM5 tethers a ternary complex containing Keap1 and Nrf2 to mitochondria. *Exp. Cell Res.* 314, 1789–1803 (2008).

42. O'Mealey, G. B. *et al.* A PGAM5-KEAP1-Nrf2 complex is required for stress-induced mitochondrial retrograde trafficking. *J. Cell Sci.* 130, 3467–3480 (2017).

43. Scheuermann, S. *et al.* Homodimerization of Amyloid Precursor Protein and Its Implication in the Amyloidogenic Pathway of Alzheimer's Disease. *Journal of Biological Chemistry* 276, 33923–33929 (2001).

44. Montagna, E. *et al.* In vivo Ca2+ imaging of astrocytic microdomains reveals a critical role of the amyloid precursor protein for mitochondria. *Glia* 67, 985–998 (2019).

45. Chiang, S. K., Chen, S. E. & Chang, L. C. The Role of HO-1 and Its Crosstalk with Oxidative Stress in Cancer Cell Survival. *Cells* 10, 2401 (2021).

46. Lee, W. S., Ham, W. & Kim, J. Roles of NAD(P)H:quinone Oxidoreductase 1 in Diverse Diseases. . 11, 1301 (2021).

47. Pan, J. X. *et al.* APP promotes osteoblast survival and bone formation by regulating mitochondrial function and preventing oxidative stress. *Cell Death Dis.* 9, (2018).

48. Wang, Y. *et al.* Lost region in amyloid precursor protein (APP) through TALEN-mediated genome editing alters mitochondrial morphology. *Sci. Rep.* 6, (2016).

49. Zheng, H. *et al.* beta-Amyloid precursor protein-deficient mice show reactive gliosis and decreased locomotor activity. *Cell* 81, 525–531 (1995).

50. Loboda, A., Damulewicz, M., Pyza, E., Jozkowicz, A. & Dulak, J. Role of Nrf2/HO-1 system in development, oxidative stress response and diseases: an evolutionarily conserved mechanism. *Cell. Mol. Life Sci.* 73, 3221 (2016).

51. Gray, J. P., Karandrea, S., Burgos, D. Z., Jaiswal, A. A. & Heart, E. A. NAD(P)H-dependent Quinone Oxidoreductase 1 (NQO1) and Cytochrome P450 Oxidoreductase (CYP450OR) differentially regulate menadione-mediated alterations in redox status, survival and metabolism in pancreatic β-cells. *Toxicol. Lett.* 262, 1 (2016).

52. Dinkova-Kostova, A. T. & Talalay, P. NAD(P)H:quinone acceptor oxidoreductase 1 (NQO1), a multifunctional antioxidant enzyme and exceptionally versatile cytoprotector. *Arch. Biochem. Biophys.* 501, 116–123 (2010).

53. He, M. *et al.* Heme oxygenase-1-derived bilirubin protects endothelial cells against high glucose-induced damage. *Free Radic. Biol. Med.* 89, 91–98 (2015).

54. Chiang, S. K., Chen, S. E. & Chang, L. C. The Role of HO-1 and Its Crosstalk with Oxidative Stress in Cancer Cell Survival. *Cells* 10, 2401 (2021).

55. Wieckowski, M. R. M. R., Giorgi, C., Lebiedzinska, M., Duszynski, J. & Pinton, P. Isolation of mitochondria-associated membranes and mitochondria from animal tissues and cells. *Nat. Protoc.* 4, 1582–1590 (2009).

56. Li, P. *et al.* The loss of cardiac SIRT3 decreases metabolic flexibility and proteostasis in an age-dependent manner. *GeroScience 2022 45:2* 45, 983–999 (2022).

57. Mendez Garcia, M. F. *et al.* Increased cardiac PFK-2 protects against high-fat diet-induced cardiomyopathy and mediates beneficial systemic metabolic effects. *iScience* 26, 107131 (2023).

Figure legends-

Figure 1. Isolated mitochondria from APP KO mice brain have impaired respiration and metabolism. (A-C). Graphs showing the state 3 respiration by utilizing different oxidizable substrates (A. Pyruvate/malate, B. glutamate/malate, C. Succinate), in the mitochondria isolated from 6-8 months old APP KO mice brain. Values shown are the means ± SD (n =4 - 6). Two-tailed paired t-test was performed for each graph, * ($P < 0.05$), ns (non-significant). **(D-E).** Graphs showing impaired electron transport chain in APP KO mitochondria as indicated by D. decreased Complex I activity as well as E. decreased NADH oxidase activity.Values shown are means ± SD (n =5 - 6). Two-tailed paired t-test was performed for each graph, * ($P < 0.05$), ns (non-significant).

Figure 2. PGAM5 and APP co-localize at the mitochondria- ER contact sites (MERCS). A. Western blot showing subcellular localization of PGAM5 and APP in wild-type (C57Bl6, 3-12 months old, females) mouse whole brain. The cellular compartments shown are Whole brain, Crude mitochondria, Mitochondria, Mitochondria-ER contact sites (MERCS) and Endoplasmic reticulum (ER). The purity of each sample was validated by its marker protein (TOM20- Mitochondria, ATPase- MERCS and BiP- ER). (**B-C).** Graphs showing western blot quantification indicating levels of B. APP protein and C. PGAM5 protein. Values shown are band intensity means ± SD (*n* =7). One-way ANOVA tests were performed for each graph, *** ($P < 0.01$), **** ($P < 0.001$), ns (non-significant).

Figure 3. PGAM5 interacts with the APP ectodomain *in vitro*. A. Schematics showing domains (GFLD; Growth-like factor domain, CuBD; Copper-binding domain, AcD; Acidic domain, ExD; Extension domain, E2, JMR; Juxtamembrane Region, TM; Transmembrane, AICD; APP intracellular domain, MM; Multimerization motif, KBD; Keap1 binding domain, PGAM; Phosphoglycerate mutase) and recombinant protein constructs (sAPPα, PGAM5-Δ90 and PGAM5-Δ54) of APP (pink) and PGAM5 (yellow). **B.** Binding curve from isothermal titration calorimetry (ITC) done using the sAPPα and PGAM5-Δ54 purified proteins (n=3). **(C-E).** Coomassie stained SDS-PAGE gels of bound and unbound material from Fc-pulldowns of C. sAPP-Fc with PGAM5Δ54 or PGAM5Δ90 purified proteins, D. sAPP-Fc, GFLD-Fc, CuBD-Fc, ExD-Fc, AcD-Fc, E2-Fc and beads with PGAM5Δ54 purified protein and E. Quantification of pull-down assays showing net PGAM5Δ54 bound and pulled down with each Fc-tagged sAPPα domain. Values shown are means ± SD (*n* =5 - 6) and the statistics were performed using Dunnett's multiple comparison test. ***** ($P < 0.0001$).

Figure 4. PGAM5 and APP interact endogenously in situ. (A-B). A. Confocal images of coronal sections of WT and APP KO mouse brain (6 months old, male) showing proximity ligation assays (PLA), done using APP and PGAM5 antibodies (APPY188, abcam, ab32136; PGAM5, abcam, ab244218). DAPI is shown in blue and PLA signal is in white. Scale bars, 20 µm. B. Plot showing PLA puncta per cell in different brain regions (CTX- Cortex, CA1- Cornu Ammonis region 1, SP- Stratum Pyramidale, SR- Stratum Radiatum, SLM- Stratum Lacunosum-Moleculare, DG- Dentate Gyrase) of WT (blue) and APP KO (red) brain sections. Values shown are the means ± SD (n = 3 images/brain region/experiment) and the statistics were performed using multiple t-tests. * (P < 0.01), nd (not detectable).

Figure 5. Transcription of Nrf2-regulated genes is altered in APP KO astrocytes. Plot showing relative mRNA expression of Nrf2-regulated genes in cultured primary astrocytes isolated from WT and APP KO mouse brains, measured by RT-qPCR. Values shown are the means ± SD (n = 8-9) and the statistics were performed using two-way ANOVA, followed by Tukey's multiple comparison test. ***** (P < 0.0001), ns (non-significant).

Figure 6. Schematic showing proposed mechanism by which APP affects Nrf2-regulated gene transcription. APP displaces Keap1 to bind to PGAM5 at the outer mitochondrial membrane. This releases Keap1-bound Nrf2 to the cytoplasm where it accumulates and eventually enters the nucleus and activates the transcription of genes to maintain normal mitochondrial function. Schematic was made in Biorender.

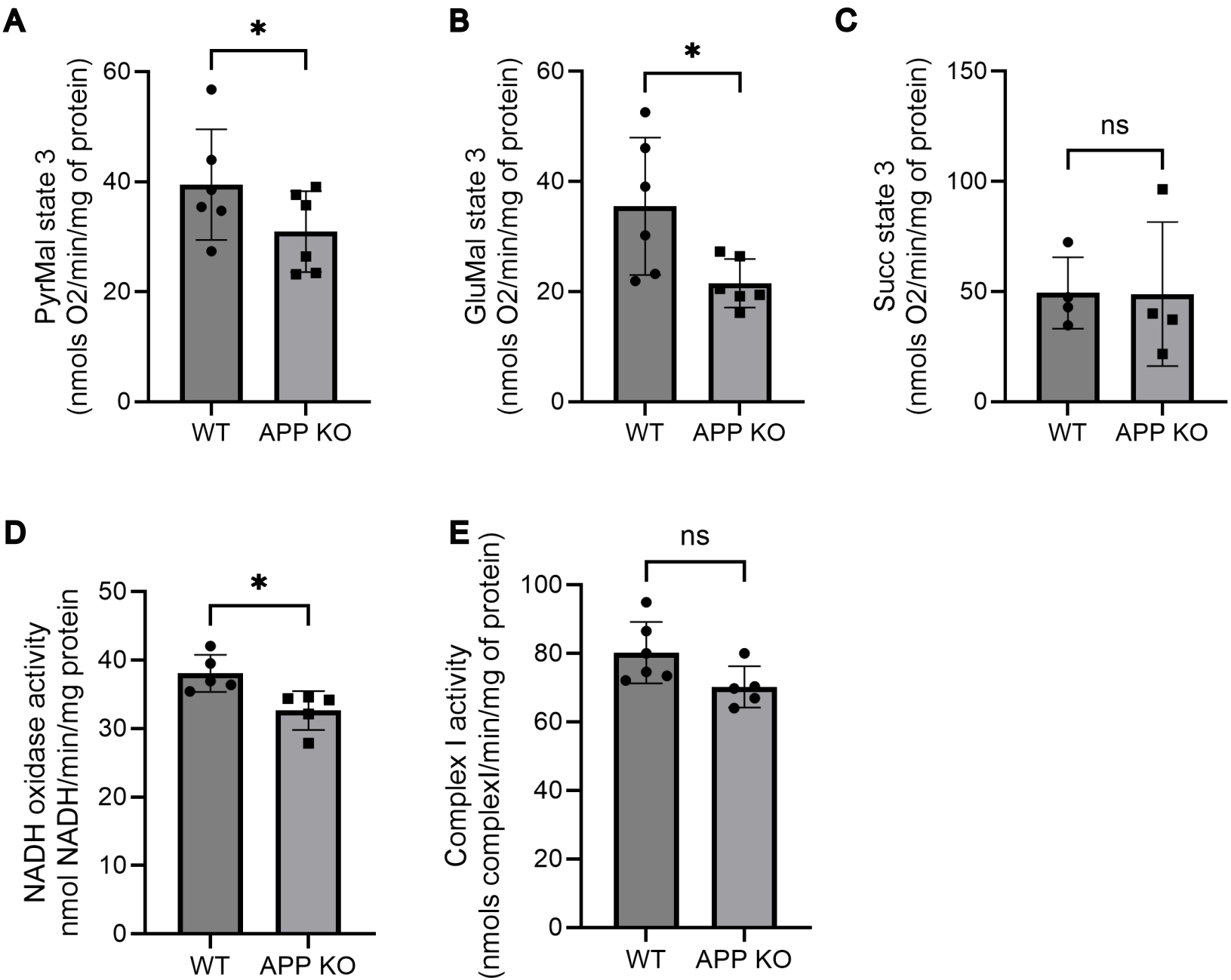
A
PyrMal state 3
(nmols O2/min/mg of protein)
60
40
20
0
*
WT
APP KO
B
GluMal state 3
(nmols O2/min/mg of protein)
60
40
20
0
*
WT
APP KO
C
Succ state 3
(nmols O2/min/mg of protein)
150
100
50
0
ns
WT
APP KO
D
NADH oxidase activity
nmol NADH/min/mg protein
50
40
30
20
10
0
*
WT
APP KO
E
Complex I activity
(nmols complexI/min/mg of protein)
100
80
60
40
20
0
ns
WT
APP KO

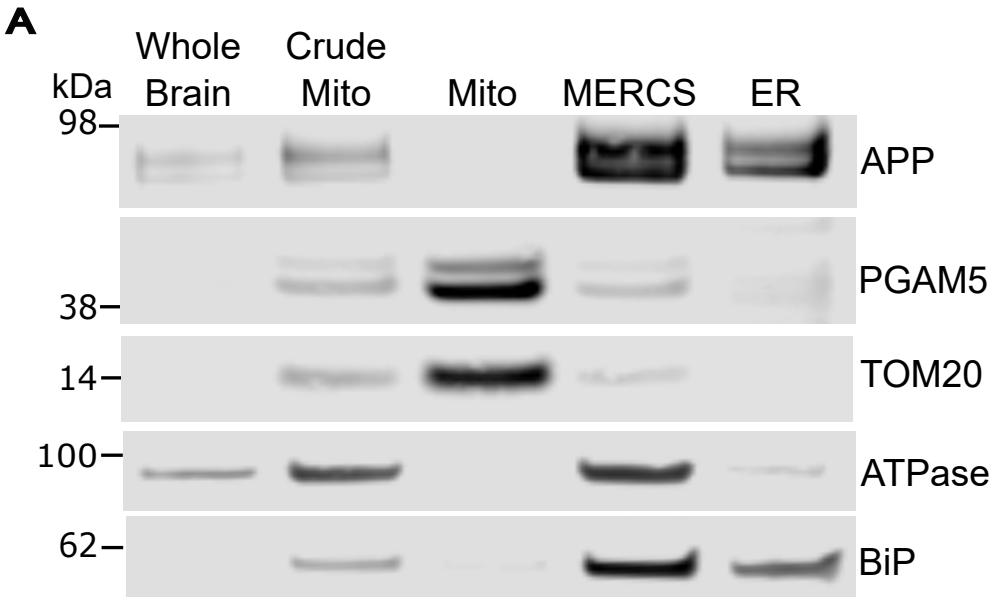
A
Whole Brain
Crude Mito
Mito
MERCS
ER
kDa
98
38
14
100
62
APP
PGAM5
TOM20
ATPase
BiP

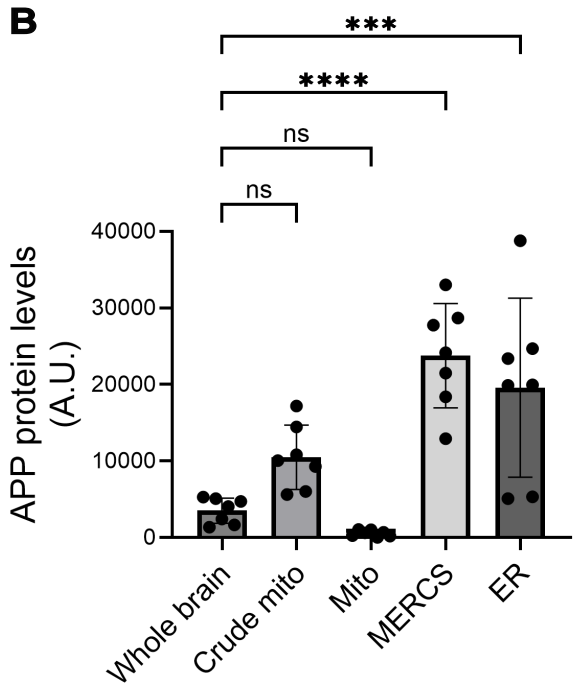
B
***
****
ns
ns
APP protein levels (A.U.)
40000
30000
20000
10000
0
Whole brain
Crude mito
Mito
MERCS
ER

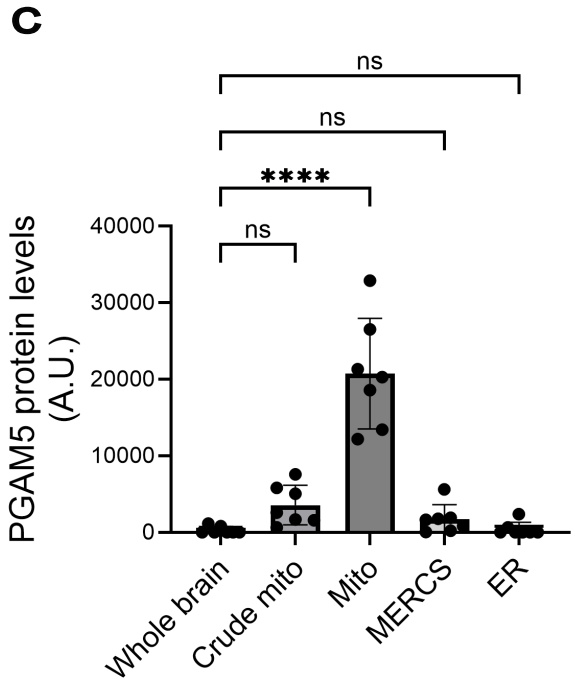
C
ns
ns
****
ns
PGAM5 protein levels (A.U.)
40000
30000
20000
10000
0
Whole brain
Crude mito
Mito
MERCS
ER

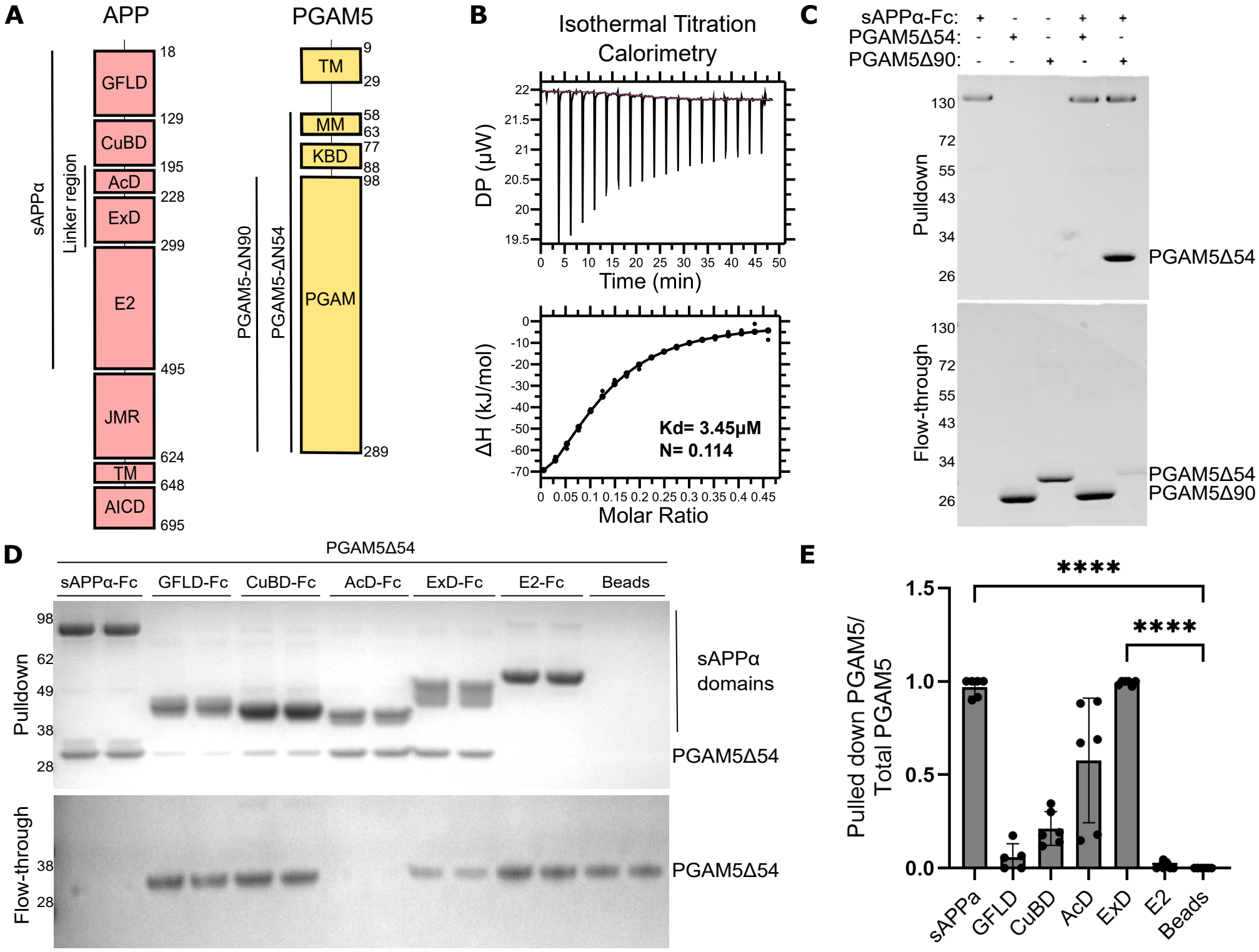
A
APP
PGAM5
GFLD
CuBD
AcD
ExD
E2
JMR
TM
AICD
sAPPα
Linker region
18
129
195
228
299
495
624
648
695
TM
MM
KBD
PGAM
PGAM5-ΔN90
PGAM5-ΔN54
9
29
58
63
77
88
98
289
B
Isothermal Titration Calorimetry
DP (μW)
Time (min)
ΔH (kJ/mol)
Molar Ratio
Kd= 3.45μM
N= 0.114
C
sAPPα-Fc:
PGAM5Δ54:
PGAM5Δ90:
Pulldown
Flow-through
PGAM5Δ54
PGAM5Δ54
PGAM5Δ90
D
PGAM5Δ54
sAPPα-Fc
GFLD-Fc
CuBD-Fc
AcD-Fc
ExD-Fc
E2-Fc
Beads
Pulldown
Flow-through
sAPPα domains
PGAM5Δ54
PGAM5Δ54
E
****
****
Pulled down PGAM5/ Total PGAM5
sAPPa
GFLD
CuBD
AcD
ExD
E2
Beads

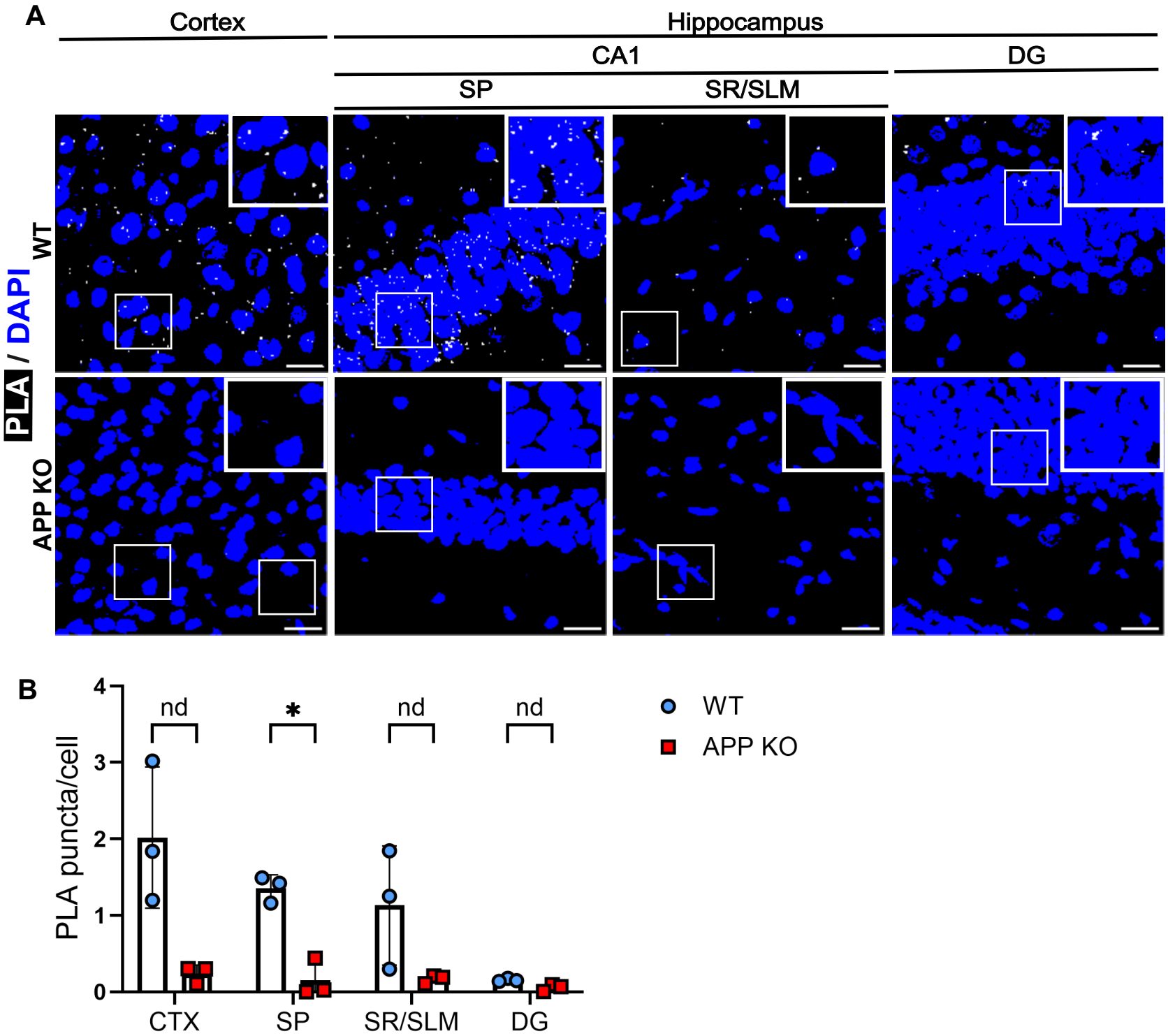
A
Cortex
Hippocampus
CA1
DG
SP
SR/SLM
WT
APP KO
PLA / DAPI
B
PLA puncta/cell
4
3
2
1
0
nd
*
nd
nd
CTX
SP
SR/SLM
DG
WT
APP KO

A.

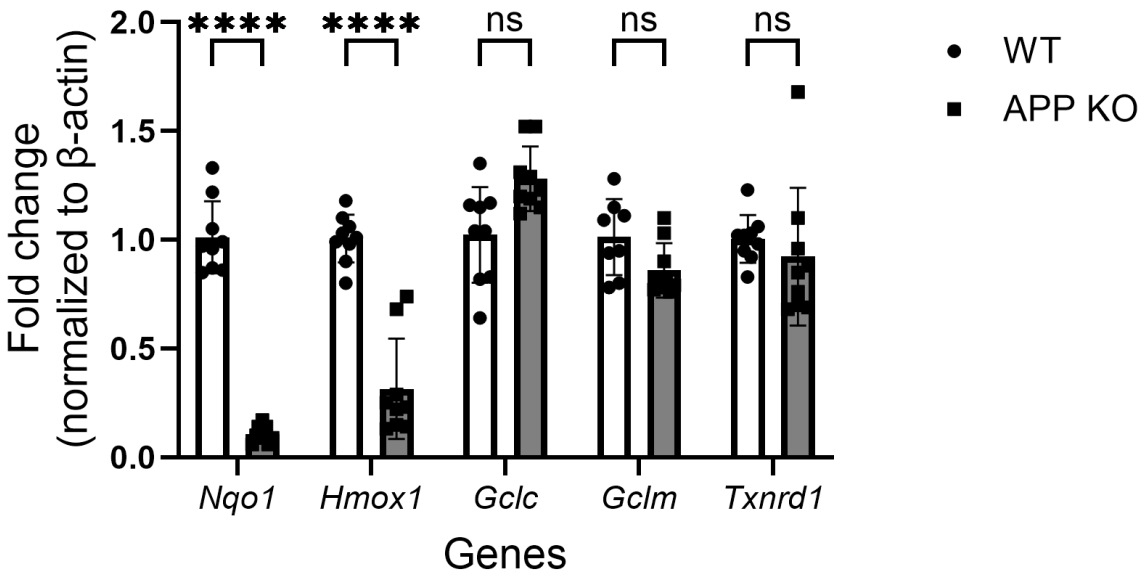
****
****
ns
ns
ns
2.0
1.5
1.0
0.5
0.0
Fold change
(normalized to β-actin)
Nqo1
Hmox1
Gclc
Gclm
Txnrd1
Genes
WT
APP KO

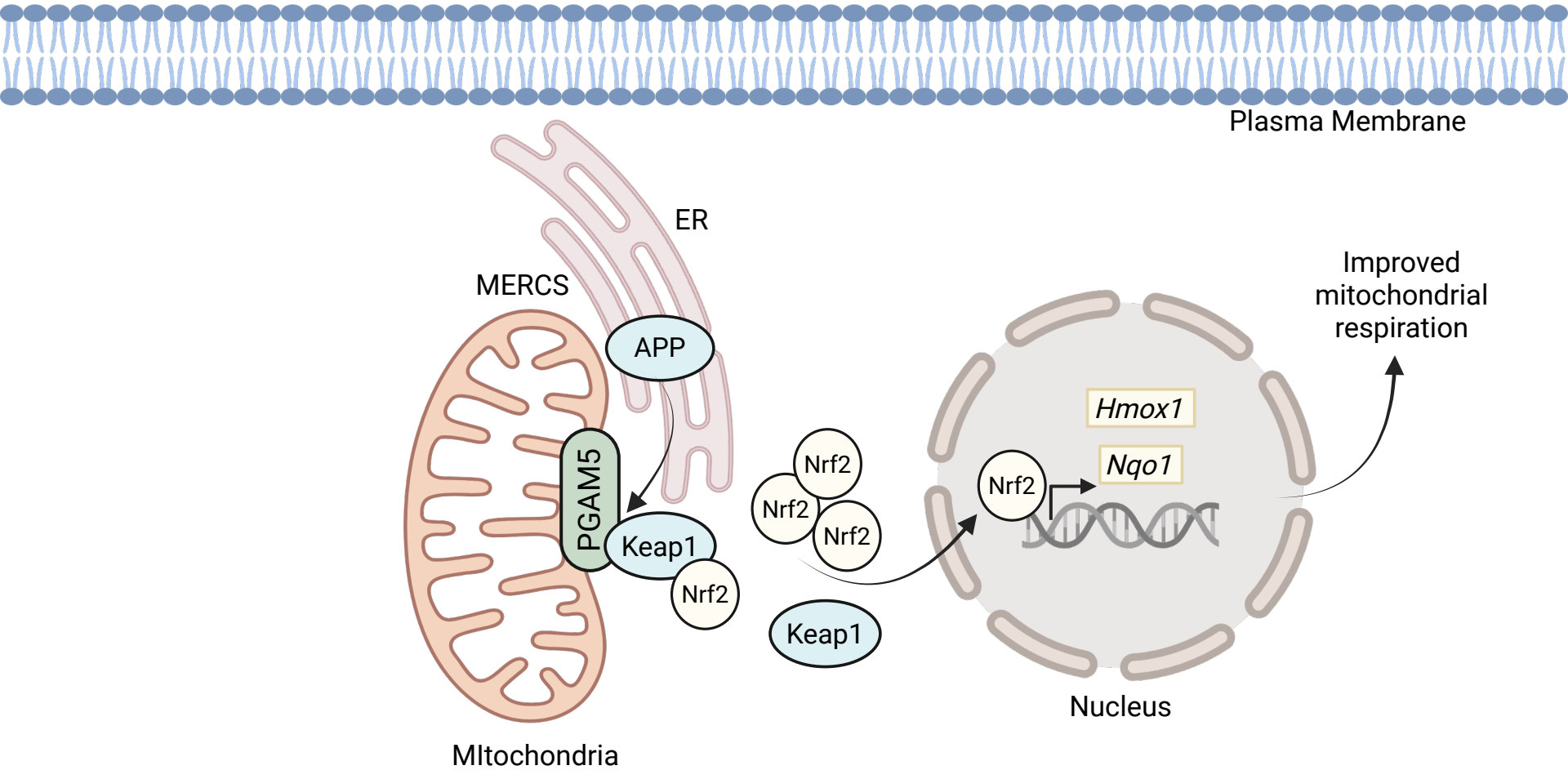
Plasma Membrane
ER
MERCS
APP
PGAM5
Keap1
Nrf2
Nrf2
Nrf2
Nrf2
Keap1
Nrf2
Hmox1
Nqo1
Improved
mitochondrial
respiration
Nucleus
MItochondria